

The effect of non-equal emission times and space-time correlations on (anti-) nuclei production

M. Kachelrieß¹, S. Ostapchenko², and J. Tjemsland¹

¹*Institutt for fysikk, NTNU, Trondheim, Norway and*

²*II. Institute for Theoretical Physics, Hamburg University, Hamburg, Germany*

(Dated: 15. March 2023)

Light (anti-) nuclei are a powerful tool both in collider physics and astrophysics. In searches for new and exotic physics, the expected small astrophysical backgrounds at low energies make these antinuclei ideal probes for, e.g., dark matter. At the same time, their composite structure and small binding energies imply that they can be used in collider experiments to probe the hadronisation process and two-particle correlations. For the proper interpretation of such experimental studies, an improved theoretical understanding of (anti-) nuclei production in specific kinematic regions and detector setups is needed. In this work, we develop a coalescence framework for (anti-) deuteron production which accounts for both the emission volume and momentum correlations on an event-by-event basis: While momentum correlations can be provided by event generators, such as PYTHIA, the emission volume has to be derived from semi-classical considerations. Moreover, this framework goes beyond the equal-time approximation, which has been often assumed in femtoscopy experiments and (anti-) nucleus production models until now in small interacting systems. Using PYTHIA 8 as an event generator, we find that the equal-time approximation leads to an error of $\mathcal{O}(10\%)$ in low-energy processes like Υ decays, while the errors are negligible at LHC energies. The framework introduced in this work paves the way for tuning event generators to (anti-) nuclei measurements.

I. INTRODUCTION

Light (anti-) nuclei are interesting particles due to their composite structure and small binding energies. This makes them ideal probes for, e.g., two-particle correlations and the QCD phase diagram in heavy ion collisions [1]. In particle collisions and decays, (anti-) nuclei can provide valuable information on the hadronisation process and momentum correlations that can be used to tune QCD inspired event generators. For the astroparticle community, the production of antinuclei is of immense interest since it is an ideal tool to search for new and exotic physics, such as dark matter annihilations or decays in the Milky Way [2–4]. In order to correctly interpret astrophysical and collider data, a description of the formation process as precise as possible is desirable.

The best motivated production model for light nuclei¹ in particle collisions—especially for small interacting systems—is arguably the coalescence model. In this model, final-state nucleons may merge if they are close in phase space. In heavy-ion collisions, the coalescence probability is often assumed to be mainly determined by the nucleon emission volume, while momentum correlations are neglected or treated as a collective effect [5, 6]. In small interacting systems, on the other hand, the coalescence condition is typically only evaluated in momentum space: For instance, in the simplest phenomenological coalescence model two nucleons merge if the momentum difference Δp in their pair rest frame is smaller than the coalescence momentum p_0 [7, 8]. However, two-

particle correlations should not be neglected in small systems because of the low multiplicities and large anti-correlations of produced nucleons [9]. It was therefore suggested in Refs. [10, 11] that the coalescence condition $\Delta p < p_0$ should be evaluated on an event-by-event basis using a Monte Carlo event generator. Moreover, the expected nucleon emission length in small interacting systems, $\sigma \simeq 1$ fm, is of the same order as the size of the wave function of the deuteron, $r_{\text{rms}}^d \simeq 2$ fm, even in point-like interactions [12] (see also Ref. [9] for an early discussion of the decay of Υ mesons). Thus, one should consider both the size of the formation region and momentum correlations on an event-by-event basis simultaneously. This is currently only achieved by the WiFunC model (Wigner Function with Correlations) introduced in Ref. [12], and further developed and discussed in Refs. [13–15]. This model is especially suitable for production processes relevant to cosmic ray interactions [13, 16, 17].

The WiFunC model, as most other sophisticated coalescence models [18–24], relies on the Wigner function approach, in which the coalescence probability is found by projecting the nucleon Wigner function onto the Wigner function of the light nucleus [6, 25–27]. One of the key advantages of this approach is the fact that the coalescence probability depends on the hadronic emission region, a quantity which can be measured in femtoscopy experiments [18]. This allows one to determine independently the free parameter of these models [14, 28, 29]. Moreover, femtoscopy experiments can be used to distinguish between the coalescence hypothesis and other formation processes like thermal freeze-out [30–36]. For instance, it was argued in Ref. [37] that the current success of the framework is a strong indication that coalescence is a major antinuclei production mechanism.

This work is structured as follows: In section II, we

¹ In the following, we denote with nuclei both nuclei and antinuclei.

review the basis of the Wigner function approach to coalescence, focusing on small interacting systems. In particular, we extend the framework to allow for non-equal emission times of the nucleons. That is, we go beyond the equal-time approximation which underlies both the experimental and theoretical framework of femtoscopy, and is expected to give up to $\mathcal{O}(30\%)$ uncertainties [37]. This effect has previously been considered in the context of heavy-ion collisions when momentum correlations can be neglected, in which case the source radius effectively is increased as $r \rightarrow r + vt$ [38–40], or using transport codes [27, 41]. In this work, however, we are interested in small interacting systems where momentum correlations should not be neglected. In section III, we review the WiFunC model and give an in-depth discussion of the choice of the nucleus wave function. Furthermore, we discuss the possibility of using the semi-classical space-time picture in QCD inspired event generators to describe the nucleon emission volume, thus allowing one to take into account space-time correlations on an event-by-event basis. Finally, in section IV, the discussions are exemplified using Pythia 8.3 [42, 43], with a focus on the equal-time approximation and the space-time picture provided by Pythia. Concretely, we consider the size of the hadronic emission region [44] (in IV A), the antideuteron spectrum [45] (in IV B), and the coalescence probability in jets [46, 47] (in IV C) measured by the ALICE collaboration. Furthermore, we compute the energy

dependence of the emission volume, predicted by Pythia in section IV D and the antideuteron production in Υ decays [48, 49] in section IV E. The examples indicate that the equal-time approximation leads to an error of $\sim 10\%$ at low energies, while the error is negligible at LHC energies. The main uncertainties of the WiFunC model and of its predictions are currently related to the accuracy of the underlying event generators for high energy collisions. Conversely, the framework allows one to use femtoscopy and antideuteron measurements to tune such event generators.

II. THE WIGNER FUNCTION APPROACH TO COALESCENCE

A. General frame-work

In femtoscopy experiments, the correlations of pairs of particles with small relative momenta are measured. Since the final-state interactions that give rise to the correlations even from an initially uncorrelated source decrease rapidly with increasing distance in phase space, we only consider the contribution from the dominant pair². The double energy spectrum can in this case be written as

$$(2\pi)^8 \gamma_1 \frac{d^6 N}{d^3 p_1 d^3 p_2} = \sum_S \int d^4 x_1 d^4 x_2 d^4 x'_1 d^4 x'_2 \rho(x_1, x_2; x'_1, x'_2) \Psi_{d,P}^{S(-)}(x_1, x_2) \Psi_{d,P}^{S(-)\dagger}(x_1, x_2), \quad (1)$$

where ρ is the two-particle density matrix of the source and $\Psi_{d,P_d}^{S(-)}(x_1, x_2) = [\Psi_{d,P_d}^{S(+)}(x_1, x_2)]^\dagger$ is the Bethe-Salpeter wave function accounting for the final-state interactions [50]. In the case of weakly bound systems such as the deuteron, helion and triton, we can connect Eq. (1) with the coalescence formalism based on generalised or relativistic Wigner functions: Neglecting the binding energy and employing the sudden approximation, the Bethe-Salpeter wave function reduces to the wave function of the static bound state. The deuteron energy spectrum can then be approximated as

$$(2\pi)^8 \gamma_d \frac{d^3 N_d}{dP_d^3} = S \int d^4 x_1 d^4 x_2 d^4 x'_1 d^4 x'_2 \rho(x_1, x_2; x'_1, x'_2) \Psi_{d,P_d}^{(-)}(x_1, x_2) \Psi_{d,P_d}^{(-)\dagger}(x_1, x_2), \quad (2)$$

where the factor $S = 3/8$ is obtained by averaging over all spin and isospin states. Note that this formula follows directly from the general rules of (relativistic) statistical quantum mechanics, if the sudden approximation is employed. The latter requires that the formation time τ of the deuteron can be neglected relative to the inverse of its binding energy E_d [51], i.e. that $\tau \ll 1/E_d \simeq 90$ fm. Factoring out then the center-of-mass motion, $\Psi_{d,P_d}^{S(-)}(x_1, x_2) = e^{iP_d X} \Psi_d^{S(-)}(x)$, one can re-write Eq. (2) as (see, e.g., Ref. [18] for details),

$$(2\pi)^8 \gamma_d \frac{d^3 N_d}{dP_d^3} = S \int d^4 r d^4 r_d d^4 q \mathcal{D}^{(4)}(q, r) W_{np}(P_d/2 + q, P_d/2 - q, r, r_d), \quad (3)$$

where

$$\mathcal{D}^{(4)}(q, r) = \int d^4 \xi e^{-iq\xi} \Psi_d^{(-)}(r + \xi/2) \Psi_d^{(-)*}(r - \xi/2) \quad (4)$$

is the (generalised or off-shell) deuteron Wigner function and W_{np} the two-nucleon Wigner function of the source. Here, r denotes the space-time distance between the nucleons, r_d the space-time position and $P_d = p_1 + p_2$ the four-momentum of the nucleus, while $q = (p_1 - p_2)/2$ is the four-momentum of the nucleons in the nucleus frame. The main

difference between Eq. (3) and the expression usually used in the literature (e.g. in Refs. [12, 18, 37]) is its time and energy dependence: The variable r_d^0 describes the “freeze-out” time of the nucleus, and does not affect the emission volume³. Meanwhile, the variable $r^0 = t$ describes the time difference in the production of the nucleons, which clearly may impact the measured emission volume. Finally, q^0 describes the off-shell structure of the two-particle system.

To proceed, it is normally assumed that the particles are produced at the same time (equal-time approximation) and/or that the source is independent of q (smoothness-approximation) [52]. However, as argued in Ref. [37], the equal-time approximation is not expected to be accurate in the case of small interacting systems. In order to check the reliability of this approximation, one should therefore go beyond the equal time approximation. As we will see, it is sufficient to assume that the particles are (approximately) on-shell when they coalesce, $W_{np} \simeq W_{np}(q^0 = 0)$. This assumption is well motivated due to the low binding energy of the antinuclei. We are in this case left with⁴

$$(2\pi)^7 \gamma_d \frac{d^3 N_d}{dP_d^3} = S \int d^4 r d^3 q \mathcal{D}_t^{(3)}(\mathbf{q}, \mathbf{r}) W_{np}^{(4)}(\mathbf{P}_d/2 + \mathbf{q}, \mathbf{P}_d/2 - \mathbf{q}, r), \quad (5)$$

where

$$\mathcal{D}_t^{(3)}(\mathbf{q}, \mathbf{r}) = \int d^3 \xi e^{-i\mathbf{q}\cdot\xi} \Psi_d^{(-)}(\mathbf{r} + \xi/2, t) \Psi_d^{(-)*}(\mathbf{r} - \xi/2, t) \quad (6)$$

is the time dependence of the static deuteron Wigner function. In the nucleus frame, this reduces to

$$\frac{d^3 N_d}{dP_d^3} = \frac{S}{(2\pi)^7} \int dt d^3 r d^3 q \mathcal{D}_t^{(3)}(\mathbf{q}, \mathbf{r}) W_{np}^{(4)}(\mathbf{q}, \mathbf{r}, t). \quad (7)$$

In order to evaluate the deuteron yield using Eq. (5), the deuteron Wigner function and the two-nucleon Wigner function have to be modelled. A key observation is that, in the classical limit, the nucleon Wigner function will reduce to the phase-space distribution. In section III, we discuss the WiFunC approach, in which the momentum correlations are provided by an event generator, while the emission volume is either assumed to be Gaussian or taken also from an event generator.

B. The effect of non-equal emission times

The various coalescence models based on the Wigner function approach differ mainly in the way how these functions are determined: In heavy-ion collisions, semi-classical transport models like the RQMD [53] or AMPT [22] schemes are used to describe the space-time evolution of the particles [27, 41]. While quantum effects are included via Pauli blocking and the stochastic nature of scatterings, the propagation of particles proceeds in these schemes classically. In contrast, many approaches which aim to describe coalescence and femtoscopy experiments in smaller interacting systems prefer to stay as long as possible within the realm of quantum mechanics. Therefore they have to rely typically on the equal-time approximation [37, 52], i.e., they assume that the particles are produced at the same time, $t = 0$. More concretely, it is assumed that $q \ll m\sigma/t \simeq 1 \text{ GeV}$ [50], where σ is the linear size of the emission volume. Since the bulk of nuclei are produced by nucleons with $q \sim \mathcal{O}(0.1) \text{ GeV}$, this condition is expected to yield an uncertainty of $\mathcal{O}(10\%)$ in pp collisions [37].

The effect of non-equal emission times on femtoscopy experiments is discussed in detail in Ref. [50], where it is shown that the relation between the Bethe-Salpeter amplitude and the corresponding non-relativistic wave function can be expressed as

$$\Psi(r) = \Psi(\mathbf{r}, t) = \int d^3 r' \delta_q(\mathbf{r} - \mathbf{r}', t) \psi(\mathbf{r}') \quad (8)$$

under the condition $q^2 \ll m^2$, which clearly is the case we are interested in. The function $\delta_q(\mathbf{r}, t)$ reduces to the ordinary Dirac delta function for $t = 0$, and for $t > 0$ it is given by [50]

$$\delta_q(\mathbf{r}, t) = \left(\frac{m}{2\pi i t}\right)^{3/2} \exp\left(\frac{i q^2 t}{2m} + \frac{i \mathbf{r}^2 m}{2t}\right). \quad (9)$$

Inserting Eq. (8) into Eq. (6) leads to

$$\mathcal{D}_t^{(3)}(\mathbf{q}, \mathbf{r}) = \mathcal{D}^{(3)}(\mathbf{q}, \mathbf{r} + \mathbf{q}t/m) \quad (10)$$

with

$$\mathcal{D}^{(3)}(\mathbf{q}, \mathbf{r}) = \int d^3 \xi e^{-i\mathbf{q}\cdot\xi} \psi(\mathbf{r} + \xi/2) \psi^*(\mathbf{r} - \xi/2). \quad (11)$$

Therefore, the deuteron yield can be expressed as

$$\frac{d^3 N_d}{dP_d^3} = \frac{S}{(2\pi)^7} \int dt d^3 r d^3 q \mathcal{D}^{(3)}(\mathbf{q}, \mathbf{r} + \mathbf{q}t/m) W_{np}^{(4)}(\mathbf{q}, \mathbf{r}, t) \quad (12)$$

in the pair rest frame. By comparing with, e.g., Refs. [12, 18, 37], one can see that non-equal emission times of the nucleons change r by the classical distance the first particle propagates before the second particle is produced. If the equal-time approximation ($t \rightarrow 0$) is applied to Eq. (12), one re-obtains, as expected, the same equation as in Refs. [12, 18, 37].

Note that four assumptions are needed to obtain Eq. (12): (1) The coalescing particles are non-relativistic

in the pair rest frame ($q^2 \ll m^2$) and (2) approximately on-shell. Moreover, (3) the wave function describing the initial and final states changes slowly compared to the interaction time (i.e., the sudden approximation) and (4) the interaction between a single pair of nucleons is dominant. All these assumptions are well motivated, and always used in the coalescence model. For example, due to the small binding energy of the deuteron, one will expect that the nucleons have to be close in phase space and approximately on-shell to coalesce.

C. Relation to femtoscopy experiments

Since the measured source function is strongly linked to the Wigner function, any coalescence model arising from Eq. (5) can be directly and independently tested and tuned by baryonic correlation experiments. Under the smoothness approximation (i.e. $W_{np}(r, r_d, P_d, q) \simeq W_{np}(r, r_d, P_d, 0)$), Eq. (5) can be written as

$$\begin{aligned} \frac{d^3 N_d}{dP_d^3} &\propto \int d^3 r dt W_{np}^{(4)}(\mathbf{r}, t) \int d^3 q \mathcal{D}_t^{(3)}(\mathbf{q}, r) \\ &= \int d^3 r |\phi(\mathbf{r})|^2 \mathcal{S}(\mathbf{r}), \end{aligned} \quad (13)$$

where $\mathcal{S}(\mathbf{r}) = W_{np}^{(3)}(\mathbf{r})$ is the emission source defined in the pair rest frame. The last equality follows directly if one in addition uses the equal-time approximation [52], $W_{np} \propto \delta(t)$. In a femtoscopy experiment, the source size $\mathcal{S}(\mathbf{r})$ can be measured via the final-state interactions encoded into the wave function $\psi(r)$ [52]. Thus, a femtoscopy experiment can be interpreted as an indirect measurement of the Wigner function. Recently, the ALICE collaboration measured the size of the baryonic emission source in pp collisions at 13 TeV, assuming an isotropic Gaussian source [44]. This measurement can be used to fix the free parameter of a coalescence model, allowing one to test and tune the coalescence models like the WiFunC model [14].

Femtoscopy experiments include often a cut in the momentum q [44]. It is thus interesting to note that it is sufficient to assume that $qt/m \ll r$ to derive Eq. (13), thereby removing the need to invoke the equal-time and smoothness approximations.

III. THE WIFUNC MODEL

In the classical limit, the nucleon Wigner function [see Eq. (12)] will describe the phase space distribution of the nucleons [54]. The main idea behind the WiFunC model is to include particle momentum correlations provided by a Monte Carlo event generator. At the same time, the nucleon emission volume can be described either by an ansatz, following general arguments regarding time and distance scales in the production process, or by the event generator. In this section, we give a short review of the

model and at the same time a deeper discussion of the choice of the nucleus wave function as well as the use of the space-time picture provided by an event generator to describe the nucleon emission volume. In particular, we comment on the consequences of the equal-time approximation [cf. Eq. (12)].

A. Deuteron wave function

In the WiFunC model, the deuteron Wigner function \mathcal{D} is an essential ingredient in the calculation of the coalescence probability. For a specific choice of the deuteron wave function ϕ , the corresponding Wigner function \mathcal{D} can be evaluated using Eq. (11). The deuteron is in a pure state, and can be well approximated by the Hulthen wave function [55]. However, it is known that the Wigner function of a pure state is strictly positive if and only if the wave function is a Gaussian [56, 57]. An interpretation of the deuteron Wigner function as a probability distribution, as it is required for the evaluation of the coalescence probability, requires therefore at first sight to use a simple Gaussian wave function, $\phi(r) \propto \exp(-r^2/2d^2)$. In this case, the Wigner function becomes

$$\mathcal{D}(r, q) = 8e^{-r^2/d^2 - d^2 q^2}. \quad (14)$$

where the choice $d = 3.2$ fm reproduces the deuteron charge radius. However, the Gaussian wave function is neither a good representation of the Hulthen wave function nor does it lead to a Wigner function which is similar to that obtained using the Hulthen wave function, cf. with Fig. 1. Thus, one should aim for a better description of the deuteron wave function.

In order to find such an improved wave function, consider now the more general pure state $\phi(r) = (\phi_r(r) + i\phi_i(r))/\sqrt{2}$, where ϕ_r and ϕ_i are real wave-functions. In this case, the Wigner function can be split into a symmetric and an antisymmetric part, $\mathcal{D}(q, r) = \mathcal{D}_r(q, r) + \mathcal{D}_i(q, r) - A(q, r)$, where \mathcal{D}_r and \mathcal{D}_i are the Wigner functions of ϕ_r and ϕ_i , respectively. The antisymmetric interference term A vanishes upon performing the integrations in Eq. (12) and will therefore not contribute to the coalescence probability. This implies that the sum of two Wigner functions from pure states can be re-cast into a Wigner function from a mixed state,

$$\begin{aligned} \mathcal{D}_r(\mathbf{q}, \mathbf{r}) + \mathcal{D}_i(\mathbf{q}, \mathbf{r}) &= \int d^3 \xi e^{-i\mathbf{q}\cdot\xi} \\ &\times \langle \mathbf{r} - \xi/2 | \left(\frac{1}{2} |\phi_r\rangle \langle \phi_r| + \frac{1}{2} |\phi_i\rangle \langle \phi_i| \right) | \mathbf{r} + \xi/2 \rangle. \end{aligned} \quad (15)$$

A particular choice is the “ ϕ_0 -fit” of Ref. [12], where the deuteron Wigner function is given by

$$\mathcal{D}(\mathbf{q}, \mathbf{r}) = 8\Delta e^{-d_1^2 q^2 - r^2 d_1^2} + 8(1 - \Delta) e^{-d_2^2 q^2 - r^2 d_2^2} - \mathcal{A}(\mathbf{q}, \mathbf{r}) \quad (16)$$

with $\Delta = 0.581$, $d_1 = 3.979$ fm, $d_2 = 0.890$ fm and \mathcal{A} is antisymmetric in \mathbf{q} and \mathbf{r} .

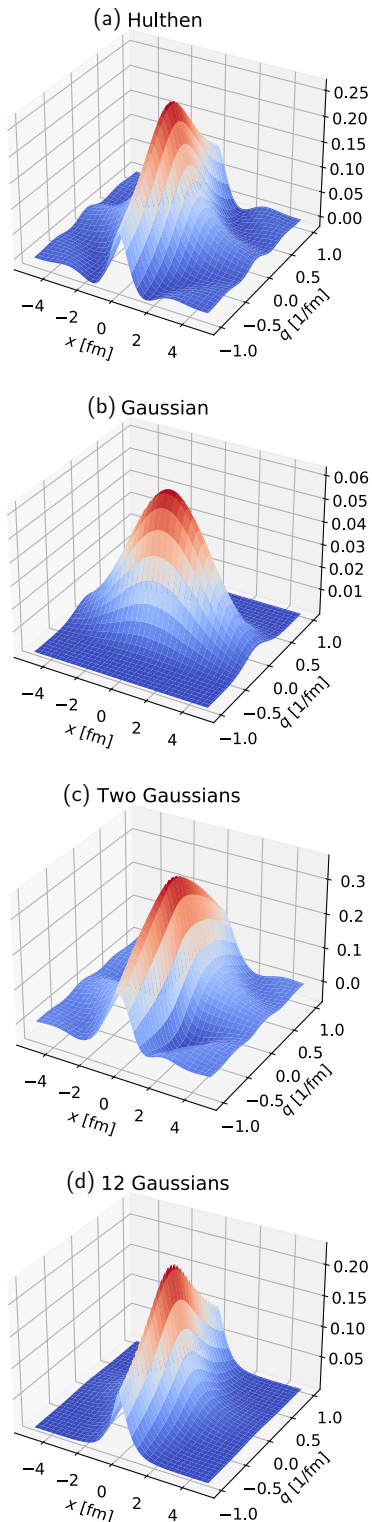


FIG. 1: The Wigner function in the (x, q_x) plane obtained numerically using (from top to bottom) (a) the Hulthen wave function, (b) a single Gaussian wave function, (c) the sum of two Gaussians with a phase shift π , and (d) the sum of 12 Gaussians. The wave functions are discussed in more detail in the text and in Ref. [12]. While it is difficult to see in the plot, the Hulthen Wigner function is symmetric, while the negative parts of the two-Gaussian Wigner function are antisymmetric.

If one describes the deuteron—incorrectly—as a mixed state, one can approximate its wave function, e.g., the Hulthen wave function, arbitrarily accurately by a sum of Gaussian states. In the fourth panel of Fig. 1, we show a one-dimensional example⁵ using 12 Gaussians whose centers are distributed evenly between $x = -5$ and $x = 5$. Since we are considering a mixed state of Gaussians, the deuteron Wigner function is itself a sum of Gaussians and strictly positive. This approach presents a clear method for handling the negative parts of the phase space distribution. However, the mixed state neglects the “quantum correlations” encoded in the Wigner function.

The negative parts of the Wigner function should vanish in the classical limit. This leads to another method of getting around the problem of a negative Wigner function: If one uses the equal-time approximation and assumes that the space and momentum distributions are uncorrelated, $W_{np} = G(\mathbf{q})H(\mathbf{r}_p, \mathbf{r}_n)$, the deuteron yield can be written as

$$\frac{d^3 N_d}{dP_d^3} = \frac{S}{(2\pi)^6} \int d^3 q G_{np}^{(3)}(\mathbf{q}) \int d^3 r_p d^3 r_n \times \mathcal{D}^{(3)}(\mathbf{q}, \mathbf{r}) H_{np}(\mathbf{r}_n, \mathbf{r}_p) \quad (17)$$

where the last integral can be interpreted at the probability density for coalescence and G_{np} is the momentum distribution provided by the event generator [12]. These are the same assumptions used in the next subsection, where H_{np} is approximated as a Gaussian. If H_{np} is sufficiently wide and well-behaved, the “probability density” will be strictly positive⁶. Thus, this may allow one to use *any* wave function and evaluate numerically the coalescence probability event-by-event. While this may work well for, e.g., high multiplicity pp collisions, the method should not be applied if position–momentum correlations are included, or the multiplicity of the interaction is small, such as in Υ decays.

In conclusion, if the deuteron wave function in the Wi-FunC model is represented by *any* $\phi(\mathbf{r}) = \phi_r(\mathbf{r}) + i\phi_i(\mathbf{r})$, where ϕ_r and ϕ_i are Gaussians centered at $r = 0$, the coalescence probability is well defined for all interactions; we suggest, with the current theoretical uncertainties, using the Wigner function in Eq. (16).

B. Nucleon distribution

Current QCD inspired event generators evaluate the parton cascade in momentum space, using a probabilistic scheme. While this is sufficient to provide two-particle momentum correlations, an extraction of the two-nucleon

⁵ See, e.g., Ref. [27] for an example in 3D.

⁶ The positivity condition depends on the shape of H_{np} and the wave function.

Wigner function W_{np} is not possible. Therefore, a semi-classical ansatz has to be made before one can evaluate the coalescence equation (12) on an event-by-event basis. In Ref. [12], the equal-time approximation was used and it was assumed that the space and momentum distributions are uncorrelated, $W_{np}(\mathbf{q}, \mathbf{P}_d, \mathbf{r}_p, \mathbf{r}_n) = G(\mathbf{q})H(\mathbf{r}_p, \mathbf{r}_n)$. In turn, the ansatz

$$H(\mathbf{r}_p, \mathbf{r}_n) = h(\mathbf{r}_p)h(\mathbf{r}_n) \quad (18)$$

with

$$h(\mathbf{r}) = (2\pi\sigma^2)^{-3/2} \exp\left(-\frac{r_\perp^2}{2\sigma_\perp^2} - \frac{r_\parallel^2}{2\sigma_\parallel^2}\right) \quad (19)$$

was used for the nucleon distributions in the laboratory (lab) frame. In particle collisions, e.g., pp , e^+e^- and pN , the longitudinal and transverse directions are defined relative to the beam direction. In annihilation and decay processes, e.g., dark matter annihilations, one should define the coordinate system relative to the initial quark–antiquark pair. With a one-Gaussian wave function, the deuteron spectrum can be written as

$$\frac{d^3N_d}{dP_d^3} = \frac{3\zeta(d)}{(2\pi)^3} \int d^3q e^{-q^2 d^2} G(\mathbf{q}), \quad (20)$$

where

$$\zeta(d) = \left[\left(\frac{d^2}{d^2 + 4\sigma_\perp^2 m_T^2/m^2} \right) \left(\frac{d^2}{d^2 + 4\sigma_\perp^2} \right) \left(\frac{d^2}{d^2 + 4\sigma_\parallel^2} \right) \right]^{1/2}. \quad (21)$$

The m_T dependence arises due to the Lorentz boost of the transverse spread from the lab frame to the pair rest frame, see Ref. [12] for details. The model can be added as an afterburner to any Monte Carlo event generator by applying the weight

$$w = 3\Delta\zeta(d_1)e^{-d_1^2 q^2} + 3(1 - \Delta)\zeta(d_2)e^{-d_2^2 q^2}, \quad (22)$$

to each nucleon pair. Here, the numerical values of the parameters are $\Delta = 0.581$, $d_1 = 3.979$ fm and $d_2 = 0.890$ fm, while m_T and q are determined event-by-event from the Monte Carlo data.

The two parameters σ_i describe the average emission length of nucleons, $\sigma_{\parallel/\perp} \simeq 1$ fm. In point-like processes, like e^+e^- collisions, the longitudinal spread is dominated by the hadronisation length, $\sigma_\parallel \sim L_{\text{had}} \simeq 1$ fm, while the transverse spread is related to Λ_{QCD} . Since they are of the same order of magnitude, it is convenient to set $\sigma = \sigma_\perp = \sigma_\parallel$. In collisions involving hadrons and nuclei, the spread will also obtain a geometrical contribution due to multiple parton–parton scatterings. In the particular case of pp collisions, the spread in the transverse and longitudinal directions are of the same size as the point-like spread [12]. Thus, one will expect $\sigma \equiv \sigma_{e^+e^-} = \sigma_{pp}/\sqrt{2}$.

The numerical value $\sigma = (1.0 \pm 0.1)$ fm has been shown to reproduce a wide range of experimental data on pp ,

e^+e^- and pN collisions, as well as baryonic femtoscopy, within experimental and theoretical uncertainties [15]. This value is also in agreement with the physical interpretation of the model, being thus a strong indication of the validity of the underlying model assumptions. The spread should in principle vary between events; in particular, it should depend on the impact parameter and multiplicity. Moreover, $\sigma_\perp \lesssim \sigma_\parallel$. With improved experimental data and improved event generators, one may have therefore to tune σ_\perp and σ_\parallel independently and vary them as a function of multiplicity.

C. Spatial correlations in event generators

Some event generators, like Pythia [42, 43] and EPOS [58, 59], include a semi-classical description of the space-time evolution of the cascade. If one employs the space-time treatment of an event generator, the coalescence weight becomes

$$w = \mathcal{D}(\mathbf{q}, \mathbf{r}) = 3 \exp\left\{-\frac{1}{d^2} \left(\mathbf{r} + \frac{\mathbf{q}t}{m}\right)^2 - q^2 d^2\right\}, \quad (23)$$

and can be extended to a two-Gaussian wave function as Eq. (2). Heisenberg's uncertainty relation limits the precision of the space-time information a specific event can contain. As a result, the space-time evolution predicted by these generators can be only an approximation to the expected probability distributions. Thus, this approach is merely a change of the semi-classical description of the nucleon distribution from that discussed in the previous subsection to that supplied by the event generator. It has, however, some advantages: First, the non-trivial Lorentz transformation of the emission volume can be taken into account in a straight-forward manner. For example, one does not have to assume that the momenta of the quark pair initiating the cascade are directed along the beam direction. Thus, more complicated processes, like $\Upsilon \rightarrow ggg$, are trivial to consider, provided that the event generator describes the process accurately. Second, the emission volume is expected to be strongly correlated with the centrality of the collision in pN and NN collisions, and thus the multiplicity. These effects can in principle be described by an event generator. Third, a weak energy dependence of the emission volume is expected. Note that these effects will likely only be visible in accelerator data, when narrow parts of the phase space are considered. In cosmic ray physics, however, it is more appropriate to use an event generator which is specialised to such applications, e.g., QGSJET [60, 61].

IV. EXAMPLES

In this section, we will be considering a few examples of antinuclei production in small interacting systems, using Pythia 8 as event generator. One should note that

the space-time treatment of parton–parton interactions in Pythia is not yet complete and there exist yet no official tunes [43]. In particular, the geometrical contribution to the longitudinal spread is not implemented, i.e., all parton–parton interactions occur at $z = 0$. As such, we cannot expect at this time Pythia to perfectly reproduce the experimental data. Nevertheless, the examples we are considering can be used to tune and develop Pythia’s space-time picture. Moreover, they will highlight some of the important features of the WiFunC model.

A. Emission volume in pp collisions at LHC

The ALICE collaboration measured recently the source radius of the baryon emission at 13 TeV in pp collisions by assuming an isotropic Gaussian source profile in the femtoscopy framework [44]. As discussed in section II C, the source radius is directly connected to the Wigner function in the coalescence model via Eq. (12). Although a simplified description of the source was used, the treatment of W_{np} in the coalescence model should reproduce this measurement. It allows us thereby to tune the coalescence model completely independently of antideuteron measurements. A caveat is that the measurement is conducted in the lab frame, while the source is defined in the pair rest frame. Therefore, the measured source size is the Euclidean distance in the lab frame at “freeze-out” boosted into the pair rest frame. This naturally explains the m_T scaling observed in Ref. [44].

In Fig. 2, we compare the $pp \otimes \bar{p}\bar{p}$ source radius measured by ALICE to that predicted by the Gaussian ansatz in the WiFunC model (see Ref. [14]) and by the space-time picture implemented in Pythia. It is clear that the qualitative behaviour of the m_T scaling is well reproduced by Pythia, while the overall source size is underestimated. The latter is expected as the longitudinal geometrical spread is not yet included in Pythia. For illustration, we have added an additional line where σ_z was increased by a factor $\sqrt{2}$; the resulting agreement indicates that the space-time picture in Pythia has the potential to reproduce the experimental data. In turn, these data can be used to tune the space-time approach of Pythia.

B. Deuteron spectrum at LHC

In Fig. 3, the deuteron spectrum in pp collisions at 0.9, 2.76, 7 and 13 TeV, as predicted by the WiFunC model with the Gaussian emission volume and with the space-time picture implemented in Pythia, is compared to the experimental data measured by the ALICE collaboration [45, 62]. It is clear that the space-time approach of Pythia is overproducing antinuclei, as expected from the under-estimated longitudinal size discussed in the previous subsection. We note again that these measurements

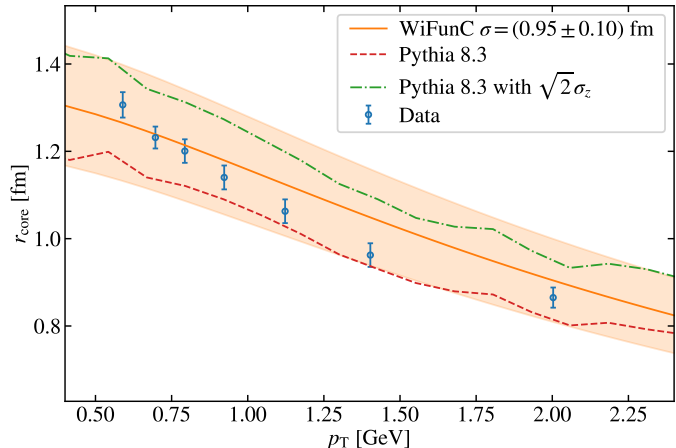


FIG. 2: The Gaussian emission size of pp and $\bar{p}\bar{p}$, r_{core} , measured by the ALICE collaboration [44] (blue circles) is compared to the prediction of the WiFunC model using the space-time picture of Pythia 8 (red dashed line) and the Gaussian ansatz for the emission volume [14] (orange solid line). Since the longitudinal geometrical spread is not yet included in Pythia, we show the results with a longitudinal spread added by hand (green dashed dotted) for visualisation.

can be used to tune Pythia’s space-time picture. Due to the composite structure of the deuteron, one can also use antinuclei experiments to tune the event generator to two-particle correlations.

The lines with and without the equal-time approximation completely overlap. That is, Pythia predicts that the inaccuracy of the equal-time approximation is negligible at LHC energies: Although the uncertainty in the emission volume in single events is of order 10%, the effect is suppressed since the coalescence condition requires the pairs of nucleons to be close-by in phase space.

C. Enhanced coalescence probability in jets

The ALICE collaboration has measured an enhanced (anti-) deuteron coalescence probability in jets [46, 47], compared to the underlying events for pp collisions at 13 TeV. More concretely, the measured coalescence factor

$$B_2 = \left(\frac{1}{2\pi p_T^{\text{deut}}} \frac{d^2 N_{\text{deut}}}{dy dp_T^{\text{deut}}} \right) / \left(\frac{1}{2\pi p_T^p} \frac{d^2 N_p}{dy dp_T^p} \right)^2 \quad (24)$$

for $p_T^p = p_T^{\text{deut}}/2$ and $|y| < 0.5$ is a factor ≈ 10 larger in a jet than in the underlying event. In the coalescence model, this is naturally explained by the larger phase space density of nucleons in the jet, and is therefore a strong indication that coalescence is a major production mechanism for deuterons. Moreover, this experiment may prove useful for understanding the exact nature of the coalescence mechanism.

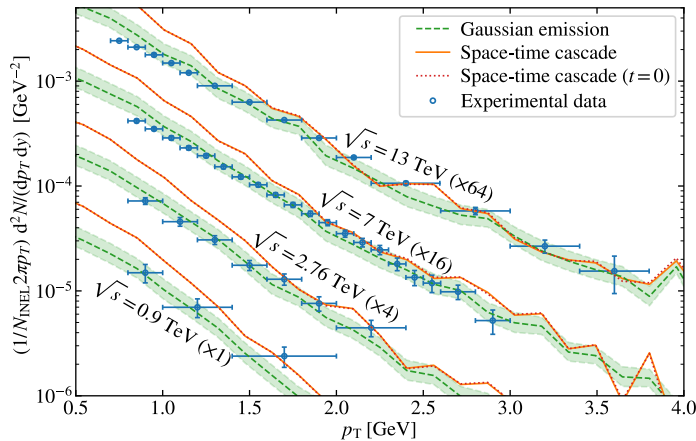


FIG. 3: The antideuteron spectrum in pp collisions at $\sqrt{s} = 0.9, 2.7, 7$ and 13 TeV, predicted by Pythia 8, using a Gaussian ansatz with $\sigma = (1.0 \pm 0.1)$ fm (green dashed line) and the space-time approach of Pythia (orange line), is compared to the experimental data of the ALICE collaboration [45, 62] (the data at 13 TeV is multiplied by a factor 0.79 to normalise the spectrum to the total number of inelastic events). The result without the equal-time approximation (red dotted line) is shown for completeness.

In Fig. 4, we compare the coalescence factor (24) predicted by the WiFunC model with a simple Gaussian ansatz (blue) and using the space-time picture in Pythia (orange). The results were obtained simulating inelastic pp collisions at 13 TeV, using Pythia 8.3 and enforcing the experimental triggers and cuts used in the event selection [46, 47]. The jet axis was approximated as the region with an azimuthal angle $|\Delta\phi| < 60^\circ$ around the so-called leading particle, as explained in Ref. [47]. Any charged particle at midrapidity ($|y| < 0.5$) and high transverse momentum ($p_T > 5$ GeV) is considered a leading particle. In the same manner, the underlying event was approximated by the region $60^\circ < |\Delta\phi| < 120^\circ$.

The overall results shown in Fig. 4 are consistent with those of Ref. [46]: There is an enhancement of a factor ~ 10 in the coalescence probability (i.e., the coalescence factor B_2) in the jet, compared to the underlying event. For comparison, we also use the simple coalescence model [46] (green) with a hard cutoff in momentum space, $p < 0.285$ GeV, and a statistical weight $3/8$. We emphasise that no fitting was performed, and the result from the WiFunC model (orange and blue) should be considered as a prediction. In accordance with Fig. 2, the space-time treatment overpredicts the coalescence probability. One should further note that the emission volume used in the simple Gaussian ansatz includes a Lorentz transformation relative to the beam axis, which is expected to be a valid approximation for a typical pp interaction. However, in Fig. 4, we are only considering events within a clear jet, in which case the boost should be done relative to the initial parton in the parton cascades. This

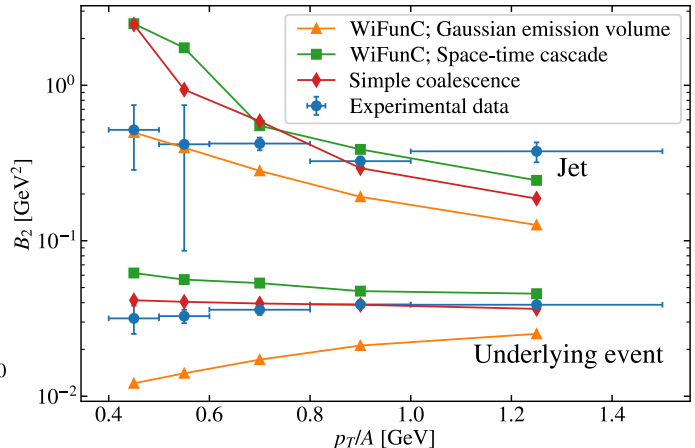


FIG. 4: The measured coalescence factor B_2 in pp collisions at $\sqrt{s} = 13$ TeV (blue circles) is compared to the predictions of Pythia 8.3 combined with the WiFunC model using a simple Gaussian ansatz (orange triangles) or based on the space-time treatment of Pythia (green squares). In addition, the results using the simple coalescence model (red diamonds) are shown for comparison.

is one of the main perks in using the space-time treatment in Pythia, since more complicated geometries are automatically taken into account.

D. Energy dependence of the emission volume

The emission volume is expected to have a weak energy dependence [12]. Within the current experimental and theoretical uncertainties, the emission volume is consistent with being constant [15]. The expected energy dependence and its relevance to coalescence is however not trivial: At high energies, the source size measured via femtoscopy experiments will increase and be much larger than 1 fm. For instance, the average Γ factor of nucleons in their pair rest-frame increases with the center-of-mass energy \sqrt{s} of the collision. As a result, the hadronisation length $\ell \simeq \Gamma/m_N$ increases with \sqrt{s} . This growth will affect mainly the longitudinal emission length. Moreover, multiple scattering in hadronic collisions enlarges the source volume additionally. While the first effect is strongly suppressed in the production of light nuclei because of the coalescence weight w , it is also suppressed in femtospectroscopy measurements because of experimental cuts. For instance, the ALICE collaboration used $q < 0.375$ GeV, in addition to the trigger condition and the rapidity cut.

In order to test this expectation and at the same time to highlight some differences between the Gaussian ansatz for the emission volume and the space-time picture of the event generator, we plot in Fig. 5 the predicted energy dependence of σ by Pythia 8.3 in pp col-

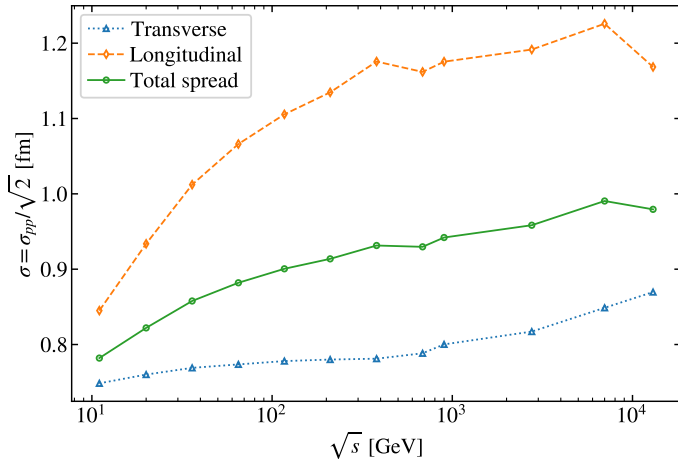
E. Υ decays

FIG. 5: The spread σ predicted by Pythia is computed as the rms value of the size of the nucleon emission region, while using the weight $\exp(-d^2q^2)$. The transverse (blue triangles), longitudinal (orange diamonds) and total (green circles) spreads are plotted as a function of the center of mass energy in pp collisions.

lisions. A weight $\exp(-d^2q^2)$ was included (q being the nucleon momentum in the pair rest frame) to highlight the “coalescence relevant” source size. Pythia predicts, as expected [12], a weak energy dependence of the emission volume and $\sigma_{\parallel} > \sigma_{\perp}$. The energy dependence can be explained by correlations between the position and momentum: Initially, the spread σ increases due to the increased energy available to the nucleons; the increase is dominated by nucleons produced back-to-back. At some point, the cut in momentum space suppresses the emission volume, making σ approximately constant.

Furthermore, there is a significant difference in the energy evolution of the spread in the longitudinal and transverse direction. In the Gaussian ansatz of the source volume [cf. with Eq. (21)], the longitudinal spread will be constant while the transverse spread will effectively be Lorentz contracted for large transverse momenta: $\sigma_{\perp} = \sigma m/m_T$. Meanwhile, using Pythia, the Lorentz boost is performed on a pair-by-pair basis and is thus not defined relative to the initial particle beam. Therefore, the expected transverse contraction in Pythia will occur both for σ_{\perp} and σ_{\parallel} .

Cosmic ray antinuclei are mainly produced by primary protons colliding with the interstellar medium at energies 10–20 GeV in the center-of-mass frame. According to the results in Fig. 5, Pythia predicts a decrease of σ by ~ 0.1 fm, when moving from LHC to such low energies. Closer to the threshold, outside the validity range of Pythia, anti-correlations can increase the baryon emission volume but will have little impact on the final deuteron spectrum since the nuclei are already suppressed by the anti-correlations in momentum. This will in any case have negligible effects on cosmic ray studies.

The decay of Υ is interesting because one can learn about the hadronisation and coalescence process at low energies. Recently, Ref. [63] systematically tested phase-space Monte Carlo models on Υ decay data. Using the WiFunC model, it was found that the emission size $\sigma \simeq 1.6$ fm—greatly larger than the expected $\simeq 1$ fm—is needed to reproduce the measured antideuteron yield. This may have three explanations [16]: (1) the WiFunC model fails, (2) the event generator over-predicts the nucleon yield or nucleon correlations, or (3) the nucleon emission volume is larger than expected in this process.

To test the first explanations, we simulate the decay of 10^7 Υ using Pythia 8.3, turning off the decay of strong resonances. In the WiFunC model with the Gaussian ansatz, we obtain⁷ $B(\Upsilon \rightarrow \bar{d}X) = 6.7_{-0.2}^{+0.1} \times 10^{-5}$ with $\sigma = (1.0 \pm 0.1)$ fm. In agreement with Ref. [63], we need $\sigma \simeq 1.5$ fm to reproduce the value measured by BaBar [48], $2.81 \pm 0.49_{-0.24}^{+0.2}$. Using the space-time treatment of Pythia, we obtain $B(\Upsilon \rightarrow \bar{d}X) = 18.0 \times 10^{-5}$, and an effective size $\sigma = 0.83$ fm. Without the equal time approximation, the result is $B(\Upsilon \rightarrow \bar{d}X) = 17.2 \times 10^{-5}$ with an effective size $\sigma = 0.93$ fm. This is a change of 4.5%. Even if the estimated emission volume in Pythia is similar to the one used in the Gaussian ansatz, the branching ratio is a factor 2–3 larger, indicating a substantial enhancement due to position and momentum correlations. In all cases, the WiFunC model over-predicts the measurement, which may well be due to uncertainties in the event generator.

In order to test the hypothesis that Pythia over-predicts the nucleon yield in the meson-to-three-gluon decay⁸, we simulate the decay of J/ψ and compare the measured branching ratio [64] of common decays into nucleons and pions⁹. The result is shown in Tab. I. As readily seen from the table, Pythia has a tendency to underestimate the branching ratio into pions, and to overestimate the branching into nucleons. This is a strong indication that Pythia over-predicts the nucleon production in J/ψ , and thus Υ decays. The nucleon yield is overproduced by a factor 2–3, implying that the deuteron yield may be overestimated by a factor 4–9.

In Pythia, the Υ meson decays mainly into three gluons, which may initiate parton showers and hadronise. In a different line of thought, the three gluons expand a triangular Lund string, and so the hadronic emission

⁷ Due to the lack of a preferred direction, we neglect the Lorentz boost in the transverse direction.

⁸ In the decay tables in Pythia, the J/ψ meson decays mainly into two gluons, even though the dominant decay channel is $J/\psi \rightarrow ggg$ [64]. We therefore change this decay channel to three gluons, like for Υ , in the simulations.

⁹ We neglect the contributions from resonances, as well as final state photons since Pythia includes Bremsstrahlung photons in the decays.

Decay	Measured value [64]	Pythia
$2(\pi^+\pi^-\pi^0)$	$(3.71 \pm 0.28) \times 10^{-2}$	2.50×10^{-3}
$3(\pi^+\pi^-\pi^0)$	$(2.9 \pm 0.6) \times 10^{-2}$	0
$\pi^+\pi^-3\pi^0$	$(1.9 \pm 0.9) \times 10^{-2}$	1.36×10^{-3}
$\pi^+\pi^-4\pi^0$	$(6.1 \pm 1.3) \times 10^{-3}$	6.5×10^{-5}
$\pi^+\pi^-\pi^0$	$(2.10 \pm 0.08) \times 10^{-2}$	1.51×10^{-2}
$2(\pi^+\pi^-\pi^0)$	$(1.61 \pm 0.20) \times 10^{-2}$	2.50×10^{-4}
$\pi^+\pi^-\pi^0 K^+ K^-$	$(1.20 \pm 0.30) \times 10^{-2}$	6.06×10^{-3}
$\pi^+\pi^-$	$(1.47 \pm 0.14) \times 10^{-4}$	7.68×10^{-3}
$2(\pi^+\pi^-)$	$(3.57 \pm 0.30) \times 10^{-3}$	5.31×10^{-3}
$\gamma 2\pi^+ 2\pi^-$	$(2.8 \pm 0.5) \times 10^{-3}$	–
$3(\pi^+\pi^-)$	$(4.3 \pm 0.4) \times 10^{-3}$	5.90×10^{-5}
$2(\pi^+\pi^-)3\pi^0$	$(6.2 \pm 0.9) \times 10^{-2}$	7.30×10^{-6}
$4(\pi^+\pi^-)\pi^0$	$(9.0 \pm 3.0) \times 10^{-3}$	0
Total	0.222 ± 0.015	0.057
$p\bar{p}$	$(2.120 \pm 0.029) \times 10^{-3}$	1.36×10^{-2}
$p\bar{p}\pi^0$	$(1.19 \pm 0.08) \times 10^{-3}$	4.31×10^{-3}
$p\bar{p}\pi^+\pi^-$	$(6.0 \pm 0.5) \times 10^{-3}$	9.07×10^{-4}
$p\bar{p}\pi^+\pi^-\pi^0$	$(2.3 \pm 0.9) \times 10^{-3}$	1.02×10^{-4}
$p\bar{n}\pi^-$	$(2.12 \pm 0.09) \times 10^{-3}$	7.47×10^{-3}
$n\bar{n}$	$(2.09 \pm 0.16) \times 10^{-3}$	1.36×10^{-2}
Total	$(1.58 \pm 0.01) \times 10^{-2}$	4.10×10^{-2}

TABLE I: Branching ratios of common J/ψ decays into pions and nucleons.

length might be substantially larger than in other processes, ~ 3 fm [9].

In conclusion, the theoretical uncertainties prevent us from presenting a conclusion about the size of the emission volume in Υ decays. The baryonic production and baryon–baryon femtoscopy measurements in Υ decays are therefore highly warranted. This will allow us, in tandem with the antideuteron data, to learn about hadronic meson decays, the hadronisation process and the coalescence process. Moreover, it may increase significantly the predictive power for some exotic antinuclei production mechanisms, such as dark matter decays or annihilation.

V. SUMMARY AND CONCLUSIONS

We have discussed the WiFunC model, a coalescence model that allows one to include momentum and spatial correlations on an event-by-event basis. Two choices for the nucleon emission volume were discussed: (1) a Gaussian ansatz, and (2) using the emission volume provided by an event generator. In the latter case, one can go beyond the equal-time approximation which until now has been invariably assumed. We have shown that this approximation leads to a $\mathcal{O}(10\%)$ uncertainty in the coalescence probability in processes close to the production threshold, such as Υ decays. The error is strongly reduced at high energies, implying that non-equal production times can be neglected for hadronic collisions at

LHC.

As concrete examples, we considered pp collisions and Υ decays, using Pythia 8. The Gaussian ansatz for the emission volume leads to a satisfactory description of the baryon emission volume and the antideuteron spectrum measured by the ALICE collaboration at LHC, while overpredicting the antideuteron production in Υ decays. We have argued, based on experimental data on nucleon production in J/ψ decays, that Pythia likely overpredicts the nucleon production in Υ decays. The space-time approach of Pythia 8, on the other hand, underpredicts the nucleon emission volume and fails to accurately describe the antideuteron spectrum. However, these deficiencies are most likely explained by the fact that the space-time treatment is not yet complete and has not yet been tuned to experimental data. Importantly, this implies that the coalescence framework introduced in this work can be used to tune the space-time treatments and momentum correlations in event generators, when comparing them to antideuteron and femtoscopy data. Once nucleon production in Υ decays is measured, one can use also antinuclei to probe the hadronisation process. In addition, we predicted the energy dependence of the emission volume using Pythia 8. This resulted, as expected, in a weak energy dependence, consistent with a constant (1.0 ± 0.1) fm within experimental and theoretical uncertainties.

This work has been motivated by an increasing amount of high-precision data on antinuclei production in small interacting systems, obtained by, e.g., the ALICE, NA61/SHINE and BELLE-II experiments. Our framework paves the way for using these antinuclei measurements to tune the space-time picture and momentum correlations in event generators used to describe these data. Improving thereby the accuracy of such generators, regarding the description of antinuclei production, may furthermore have an important impact on predictions of antinuclei production by cosmic rays and dark matter.

Note added: While finalising this manuscript, the related work [65] appeared on the arxiv. The authors of that work employ the equal-time approximation together with Eq. (17) and a Gaussian ansatz for H_{np} . The width of the Gaussian was however treated as a variable, $\sigma \rightarrow \sigma(\mathbf{r}, t)$, what is inconsistent with the assumptions needed to derive the deuteron yield in Eq. (17). We also note that our results for the emission volume, based on Pythia 8, are in disagreement with theirs: We obtain with Pythia a source size which decreases with transverse mass—in agreement with the experimental data—while the source size derived in Ref. [65] increases. This discrepancy is likely mainly caused by a different interpretation of the effect of the equal-time approximation in a femtoscopy experiment: In deriving the core size shown in Fig. 2, we enforce $t = 0$ in the lab frame. Meanwhile, Ref. [65] enlarges the emission volume by propagating the produced particles until $t = 0$.

VI. ACKNOWLEDGEMENTS

This work benefited from discussions at the workshop “Antinuclei in the Universe” at the Munich Institute for Astro- and Particle Physics (MIAPP) which is

funded by the Deutsche Forschungsgemeinschaft (DFG, German Research Foundation) under Germany’s Excellence Strategy – EXC-2094 – 390783311. S.O. acknowledges support from the Deutsche Forschungsgemeinschaft (project number 465275045).

-
- [1] H. Caines, Nucl. Phys. **A967**, 121 (2017).
- [2] P. Chardonnet, J. Orloff, and P. Salati, Phys. Lett. **B409**, 313 (1997), astro-ph/9705110.
- [3] F. Donato, N. Fornengo, and P. Salati, Phys. Rev. **D62**, 043003 (2000), hep-ph/9904481.
- [4] P. von Doetinchem et al., JCAP **08**, 035 (2020), 2002.04163.
- [5] L. Csernai and J. I. Kapusta, Phys. Rept. **131**, 223 (1986).
- [6] J. L. Nagle, B. S. Kumar, D. Kusnezov, H. Sorge, and R. Mattiello, Phys. Rev. C **53**, 367 (1996).
- [7] A. Schwarzschild and C. Zupancic, Phys. Rev. **129**, 854 (1963).
- [8] S. T. Butler and C. A. Pearson, Phys. Rev. **129**, 836 (1963), ISSN 0031-899X.
- [9] G. Gustafson and J. Hakkinen, Z. Phys. C **61**, 683 (1994).
- [10] L. A. Dal, Master’s thesis, NTNU Trondheim, available at <http://hdl.handle.net/11250/246403> (2011), URL <http://hdl.handle.net/11250/246403>.
- [11] M. Kadastik, M. Raidal, and A. Strumia, Phys. Lett. **B683**, 248 (2010), 0908.1578.
- [12] M. Kachelrieß, S. Ostapchenko, and J. Tjemsland, Eur. Phys. J. **A56**, 4 (2020), 1905.01192.
- [13] M. Kachelrieß, S. Ostapchenko, and J. Tjemsland, JCAP **08**, 048 (2020), 2002.10481.
- [14] M. Kachelrieß, S. Ostapchenko, and J. Tjemsland, Eur. Phys. J. A **57**, 167 (2021), 2012.04352.
- [15] J. Tjemsland, PoS **TOOLS2020**, 006 (2021), 2012.12252.
- [16] M. Kachelrieß, S. Ostapchenko, and J. Tjemsland, Comput. Phys. Commun. **287**, 108698 (2023), 2206.00998.
- [17] L. Šerkšnytė et al., Phys. Rev. D **105**, 083021 (2022), 2201.00925.
- [18] R. Scheibl and U. W. Heinz, Phys. Rev. **C59**, 1585 (1999), nucl-th/9809092.
- [19] K.-J. Sun, L.-W. Chen, C. M. Ko, J. Pu, and Z. Xu, Phys. Lett. B **781**, 499 (2018), 1801.09382.
- [20] K.-J. Sun, L.-W. Chen, C. M. Ko, and Z. Xu, Phys. Lett. B **774**, 103 (2017), 1702.07620.
- [21] T. Shao, J. Chen, C. M. Ko, and K.-J. Sun, Phys. Lett. B **801**, 135177 (2020), 1910.14281.
- [22] K.-J. Sun and C. M. Ko, Phys. Rev. C **103**, 064909 (2021), 2005.00182.
- [23] W. Zhao, K.-j. Sun, C. M. Ko, and X. Luo, Phys. Lett. B **820**, 136571 (2021), 2105.14204.
- [24] T. Shao, J. Chen, Y.-G. Ma, and Z. Xu, Phys. Rev. C **105**, 065801 (2022), 2205.13626.
- [25] M. Gyulassy, K. Frankel, and E. a. Remler, Nucl. Phys. A **402**, 596 (1983).
- [26] P. Danielewicz and G. Bertsch, Nucl. Phys. A **533**, 712 (1991).
- [27] R. Mattiello, H. Sorge, H. Stoecker, and W. Greiner, Phys. Rev. C **55**, 1443 (1997), nucl-th/9607003.
- [28] K. Blum, K. C. Y. Ng, R. Sato, and M. Takimoto, Phys. Rev. **D96**, 103021 (2017), 1704.05431.
- [29] K. Blum and M. Takimoto, Phys. Rev. C **99**, 044913 (2019), 1901.07088.
- [30] S. Acharya et al. (ALICE), Nucl. Phys. A **971**, 1 (2018), 1710.07531.
- [31] A. Andronic, P. Braun-Munzinger, K. Redlich, and J. Stachel, Nature **561**, 321 (2018), 1710.09425.
- [32] V. Vovchenko, B. Dönigus, and H. Stoecker, Phys. Lett. B **785**, 171 (2018), 1808.05245.
- [33] F. Bellini and A. P. Kalweit, Phys. Rev. C **99**, 054905 (2019), 1807.05894.
- [34] J. Chen, D. Keane, Y.-G. Ma, A. Tang, and Z. Xu, Phys. Rept. **760**, 1 (2018), 1808.09619.
- [35] X. Xu and R. Rapp, Eur. Phys. J. A **55**, 68 (2019), 1809.04024.
- [36] D. Oliinychenko, L.-G. Pang, H. Elfner, and V. Koch, Phys. Rev. C **99**, 044907 (2019), 1809.03071.
- [37] F. Bellini, K. Blum, A. P. Kalweit, and M. Puccio, Phys. Rev. C **103**, 014907 (2021), 2007.01750.
- [38] S. Mrowczynski, Phys. Lett. B **277**, 43 (1992).
- [39] R. Lednický, V. L. Lyuboshits, B. Erazmus, and D. Nouais, Phys. Lett. B **373**, 30 (1996).
- [40] R. Maj and S. Mrowczynski, Phys. Rev. C **80**, 034907 (2009), 0903.0111.
- [41] J. L. Nagle, B. S. Kumar, M. J. Bennett, G. E. Diebold, J. K. Pope, H. Sorge, and J. P. Sullivan, Phys. Rev. Lett. **73**, 1219 (1994).
- [42] C. Bierlich et al. (2022), 2203.11601.
- [43] S. Ferreres-Solé and T. Sjöstrand, Eur. Phys. J. C **78**, 983 (2018), 1808.04619.
- [44] S. Acharya et al. (ALICE), Phys. Lett. B **811**, 135849 (2020), 2004.08018.
- [45] S. Acharya et al. (ALICE), Phys. Rev. C **97**, 024615 (2018), 1709.08522.
- [46] ALICE collaboration (ALICE) (2022), 2211.15204.
- [47] S. Acharya et al. (ALICE), Phys. Lett. B **819**, 136440 (2021), 2011.05898.
- [48] J. P. Lees et al. (BaBar), Phys. Rev. D **89**, 111102 (2014), 1403.4409.
- [49] D. M. Asner et al. (CLEO), Phys. Rev. D **75**, 012009 (2007), hep-ex/0612019.
- [50] R. Lednický, Phys. Part. Nucl. **40**, 307 (2009), nucl-th/0501065.
- [51] L. Schiff, *Quantum Mechanics* (McGraw-Hill, New York, 1963).
- [52] M. A. Lisa, S. Pratt, R. Soltz, and U. Wiedemann, Ann. Rev. Nucl. Part. Sci. **55**, 357 (2005), nucl-ex/0505014.
- [53] H. Sorge, H. Stoecker, and W. Greiner, Nucl. Phys. A **498**, 567C (1989).
- [54] W. B. Case, American Journal of Physics **76**, 937 (2008), <https://doi.org/10.1119/1.2957889>, URL <https://doi.org/10.1119/1.2957889>.
- [55] V. I. Zhaba (2017), 1706.08306.
- [56] R. Hudson, Reports on Mathematical Physics

- 6**, 249 (1974), ISSN 0034-4877, URL <https://www.sciencedirect.com/science/article/pii/003448777490007X>.
- [57] F. Soto and P. Claverie, Journal of Mathematical Physics **24**, 97 (1983), <https://doi.org/10.1063/1.525607>, URL <https://doi.org/10.1063/1.525607>.
- [58] K. Werner, F.-M. Liu, and T. Pierog, Phys. Rev. C **74**, 044902 (2006), hep-ph/0506232.
- [59] T. Pierog, I. Karpenko, J. M. Katzy, E. Yatsenko, and K. Werner, Phys. Rev. C **92**, 034906 (2015), 1306.0121.
- [60] S. Ostapchenko, Phys. Rev. **D83**, 014018 (2011), 1010.1869.
- [61] S. Ostapchenko, EPJ Web Conf. **52**, 02001 (2013).
- [62] S. Acharya et al. (ALICE), Eur. Phys. J. C **80**, 889 (2020), 2003.03184.
- [63] D. Marietti, A. Pilloni, and U. Tamponi (2022), 2208.14185.
- [64] R. L. Workman et al. (Particle Data Group), PTEP **2022**, 083C01 (2022).
- [65] M. Horst, L. Barioglio, F. Bellini, L. Fabbietti, C. Pinto, B. Singh, and S. Tripathy (2023), 2302.12696.